Geophysical Research Letters

Supporting Information for

Volumetric solid concentration as a main proxy for basal force fluctuations generated by highly concentrated sediment flows

Marco Piantini[1,2], Florent Gimbert[1], Evangelos Korkolis[1], Romain Rousseau[2], Hervé Bellot[2], and Alain Recking[2]

[1]University Grenoble Alpes, CNRS, IRD, Institute for Geosciences and Environmental Research (IGE), Grenoble, France

[2] University Grenoble Alpes, INRAE, ETNA, Grenoble, France

Contents of this file

Additional Supporting Information (Files uploaded separately)

Introduction

In text S1 we give supplementary information about the installation of the piezoelectric sensors and the installation and calibration of the force plate and sensor. In text S2 we provide specific information on how we estimate the volumetric solid concentration and the downstream particle and sediment flow velocity. In text S3 we show the results of a supplementary experiment carried out to investigate the seismic signature of different particle impacts on the flume. In text S4 we show the uncertainties in flow properties measurements at the beginning of the highly concentrated sediment flow. In text S5 we show other experiments not presented in the main manuscript. In text S6 we show the control of the coarse fraction of the sediment mixture on force fluctuations through applying a simplified framework from the model of Tsai et al. (2021). Finally, in text S7, we show the relationships between flow properties and force power by changing the moving average window size for the experiments presented in the main manuscript.

Text S1. Installation of the piezoelectric sensors and force plate and sensor

The piezoelectric sensors are mounted on the outside of one of the sidewalls of the channel, using mounting brackets and double-sided adhesive tape (Figure S1a). The force plate and force sensor have been installed to maximize its isolation from external flume vibrations. The force plate is supported by the two force sensors (Figure S1b), which in turn rest on a steel support piece that is mechanically connected to the channel substructure (Figure S1a and Figure S1b). The stiffness of the support piece is high enough to consider that all impacts on the force plate are totally transmitted to the force sensors. As the flume rests on a substructure, shock absorbers are placed between the flume and the substructure to avoid the transmission of vibration to the force sensors from the substructure (Figure S1c). The force plate and the rest of the flume bed are connected by 5 mm-long seals (Figure S1d). To ensure continuity with the channel bed roughness, we cover with silicone and sediments the seals and the force plate like the rest of the channel bed (Figure S1e). The force sensors have been fitted under a preload of 25 kHz to ensure measurements stability and linearity between the applied load and the sensor output.

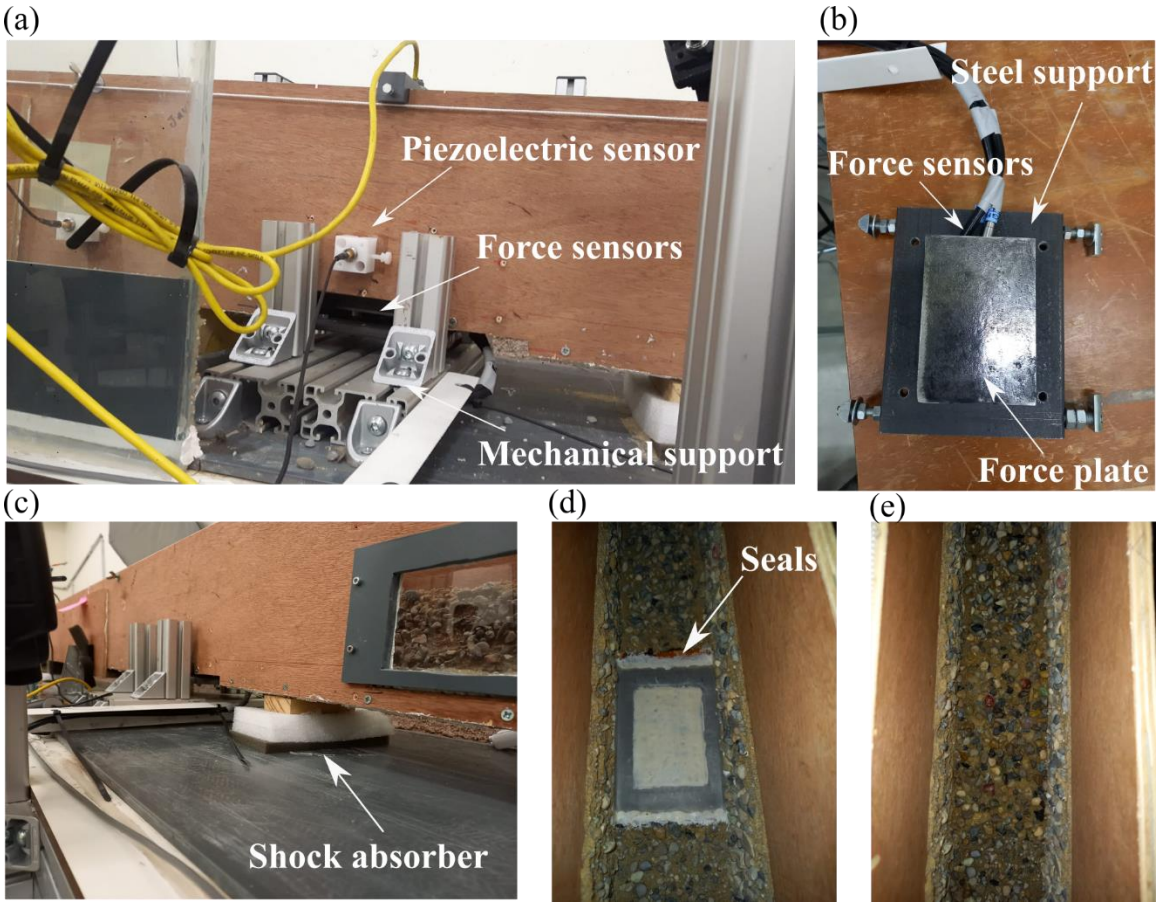

Figure S1. (a-e) Photos of the experimental setup and instruments. (a) Side view of the piezoelectric sensor mounted on the flume sidewall. Below are the different parts installed for the force measurements, i.e. the force sensors and their supports. (b) Photo of the force sensors, force plate, and steel support before installation. (c) Side view of the flume with shock absorbers between the channel bed and substructure. (d) Top view over the force plate. Lateral seals are visible. (e) Top view over the force plate after adding silicone and sediments.

Text S2. Estimations of volumetric solid concentration and particle and sediment flow velocity

We estimate the bulk density of the sediment flows following Iverson et al. (2010):

$$\rho(t) \approx \frac{\sigma_{bed}(t)}{gh(t)cos\theta} \quad (1)$$

where σ_{bed} is the mean basal normal stress, i.e. the mean basal normal force divided by the area of the force plate, g is acceleration due to gravity, $h(t)$ is the flow surface elevation, and θ is the channel slope. We assume that the mean basal normal stress balances the slope-normal static weight of the flow, which is totally supported by the force plate. From the bulk density estimation, the volumetric solid concentration can be computed as follow:

$$\phi(t) = 1 - \frac{\rho_{water}}{\rho(t)} \quad (2)$$

We estimate the macroscopic velocity of the highly concentrated sediment flow (U_x) in three different ways: (i) by tracking the flow through the cameras installed along the channel; (ii) by evaluating time delays in the surface flow elevation measurements; (iii) by evaluating time delays in the seismic measurements. If one of the three estimations differ from the others by $\pm 50\%$, we consider it incorrect and we compute the average of the remaining ones. We also estimate the local downstream velocity of individual particles in the upper part of the flow (u_x) by manually tracking their displacement between consecutive frames taken by the upstream camera. We consider the biggest particles of the sediment mixture for practical reasons, as they are coloured in blue and therefore easy to identify, and because they play a major role in generating seismic vibrations through highly energetic impacts (Tsai et al., 2012).

Text S3. The sensitivity of the piezoelectric sensors to particle impacts

We carry out specific experiments to investigate the sensitivity of the piezoelectric sensors to different mechanisms potentially generating flume vibrations such as particle impacts on the bed and on the sidewalls. To do so we drop a pebble of known mass ($m = 6.6$ g) from a fixed height ($z = 5$ cm) and we use a hand-made pendulum that allows for the same force impact on the sidewall where the sensor is installed. We produce three identical impacts at the same section and then we compute the power spectral density with the Welch's method. In Figure S2 we show the seismic power of the average over the three impacts. We observe that impacts on

the sidewall dominate over impacts on the bed in the whole frequency range, but this difference is significant especially at high frequency (over 2500 Hz).

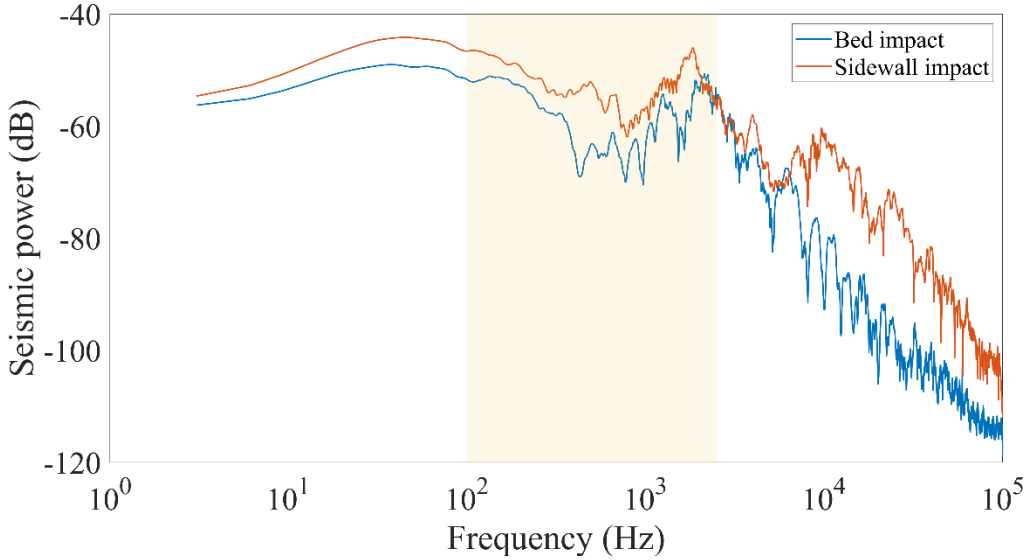

Figure S2. Seismic power as a function of frequency for the impact to the bed (blue curve) and to the sidewall (orange curve). The brownish area shows the frequency range chosen for the analysis.

Text S4. Uncertainties in flow properties measurements at the beginning of the highly concentrated sediment flow

The very first seconds of phase II are characterized by a different relationship between the investigated flow properties and force power compared to the rest of the highly concentrated sediment flow (Figure 3b-c-d and Figure 3f-g-h). A similar behaviour was observed by Allstadt et al. (2020), who pointed out that the unsaturated flow front showed a different link with basal force fluctuations compared to denser parts of the debris flow. It may indicate that below a certain value, an increased bulk density coincides with higher particle impact rate to the bed, leading to stronger force fluctuations as hypothesized by existing theoretical models (Farin et al., 2019; Tsai et al., 2012). However, we must acknowledge that in our setup there exist uncertainties on flow properties computations within this early stage of phase II. Indeed, the video recordings reveal that sometimes clusters of sediments get stuck along the channel (as presented by Piantini et al. (2021)) just before the development and passage of the denser flow.

When occurring above the force plate, these temporal depositions affect the measurements, leading to incorrect conclusions since they do not reflect the dynamics of phase II.

Text S5. Additional experiments

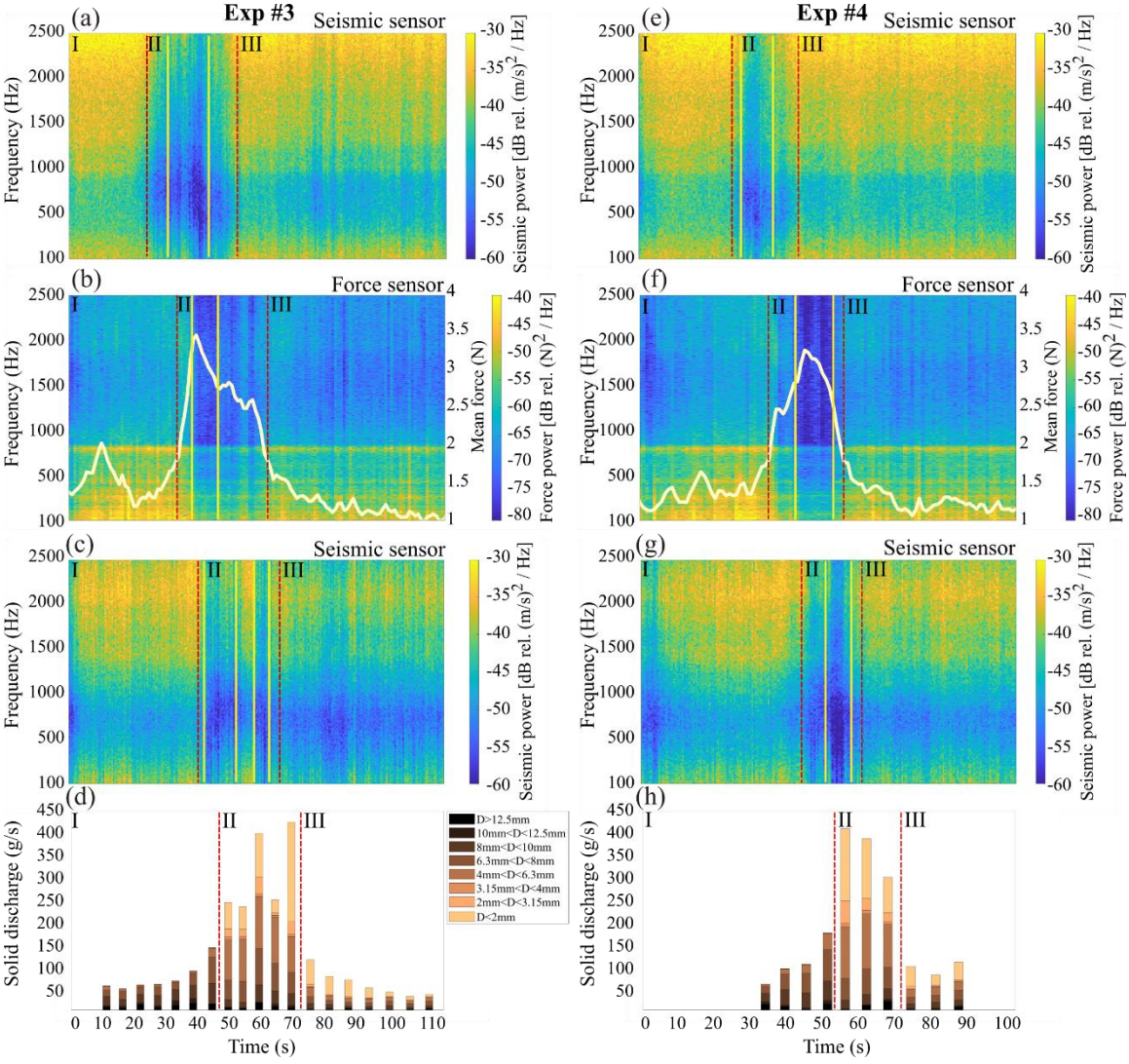

Figure S3. (a-c) and (e-g) Seismic power detected by the upstream and downstream seismic sensor, respectively. It is shown as a function of time and frequency; different colours refer to different levels of power. (b-f) Force power detected by the force sensor. We note that a band of resonance is visible around 1000 Hz. (d-h) Outlet sediment flux measurements. Each coloured bar refers to the particle diameter displayed in the legend, while the bar length is proportional to the percentage in weight of the related size. It's worth recalling that the absence of sediment flux measurements does not necessarily correspond to zero sediment flux, as measurements are by hand and not continuous in time. The vertical dashed red lines divide the three different phases, while the yellow squares delimit the time interval with the maximum content of fine sediments in phase II.

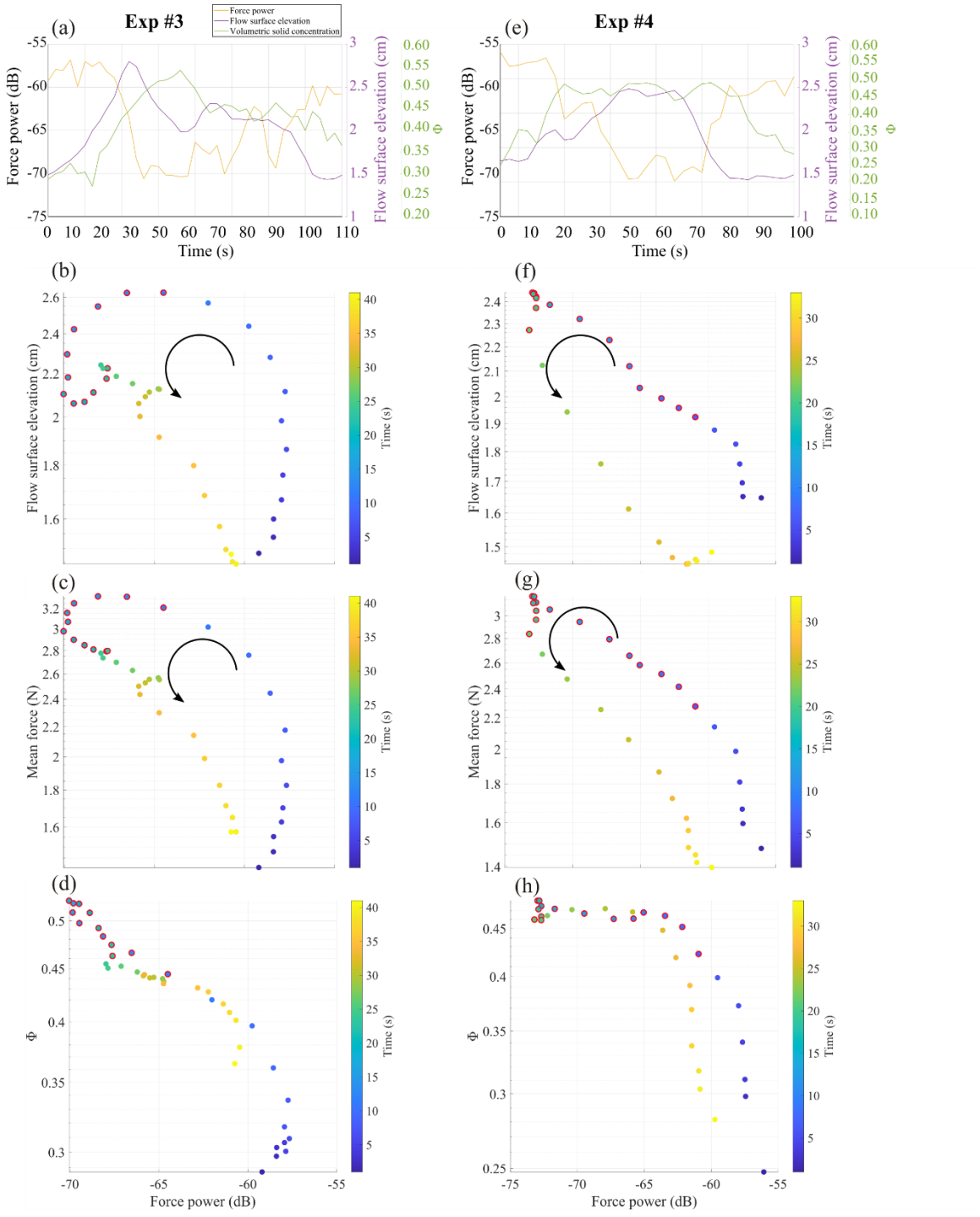

Figure S4. All the panels of Figure S4 refer to the time intervals between the vertical dashed red lines in Figure S3b and S3f. Figure S4a and S4e show the evolution in time of the force power, flow surface elevation, and volumetric solid concentration associated with the highly concentrated sediment flows, while the log-log scatterplots of Figure S4b-c-d and Figure S4f-g-h have force power on the x axis and flow properties on the y axis, where dots' color changes with time. As stated in the main text, we are able to identify the time interval when the content

of fine sediments is maximum. These moments are marked in the scatterplots with circled dots. All the measurements are smoothed on a time window of 5 sec.

Text S6. The control of the coarse fraction of the sediment mixture on force fluctuations

Tsai et al. (2012) propose that the seismic signal P generated by a sediment flow is directly related to two main geometric parameters of the flux, i.e. the number of particles n and the mass m (i.e. the diameter) of them, and two dynamic parameters, which are the rate of impact $1/t_i$ and the impact velocity w_i. Their model can be written as:

$$P \sim \frac{n}{t_i} m^2 w_i^2 \quad (1)$$

The model is built under simplistic assumptions, but it can be adopted to better understand the influence of each of these parameters on the generation of seismic power. As we are interested in investigating the role of the particle diameter, we express the seismic power as a function of the mass, under the assumption that the other parameters (i.e. n, $1/t_i$, and w_i) do not depend on the grain size. If we further consider that the mass of the particle is proportional to the third power of the particle diameter, we can rewrite equation 1 in the form:

$$P = \int p(D)\, D^6 dD \quad (2)$$

where p(D) is the percentage of grains of diameter D. The seismic power for phase I, II, and III is shown in Figure S7. We can observe that in the frequency range of interest ($100 - 2500$ kz) the coarse fraction of the sediment flow generates most of the seismic power. For each phase most part of the seismic power is always related to the coarse fraction of the flux. Although phase II can reach high contents of fines (~ 30 %), their contribution to seismic power is low. The contribution of particle diameters of 4 mm is 12 dB lower than that of particles of 8 mm.

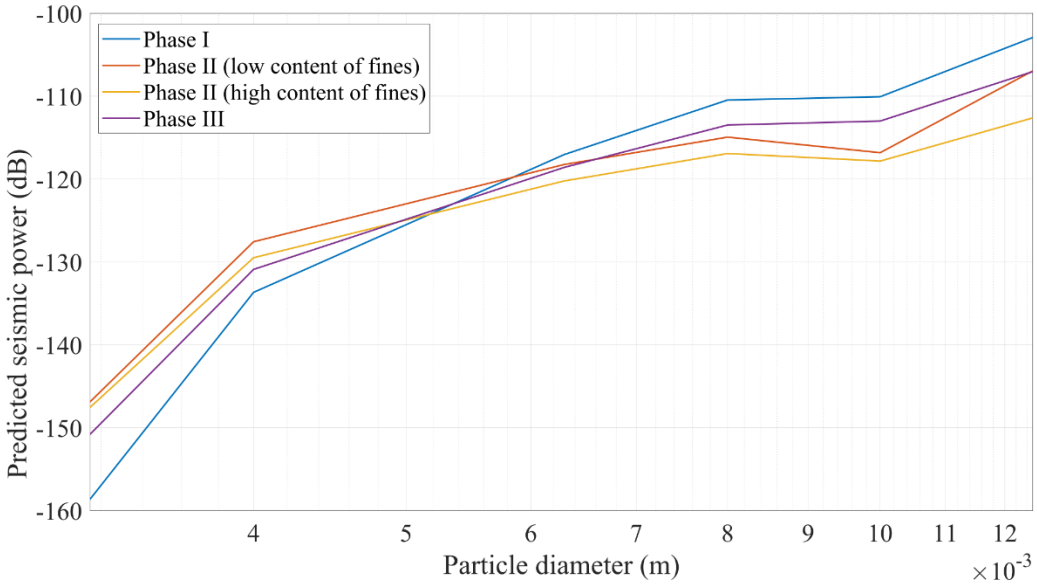

Figure S5. Predicted seismic power as a function of particle diameter following Tsai et al. (2012). Predictions are shown for each phase in a log-log plot. Particle diameters are truncated at 3.15 mm since the contribution of smaller particles is negligible.

Text S7. Changing the moving average window size

In Figure S6 we show the equivalent of Figure 3 from the main text but with a moving average window size of 2 s instead of 5 s. We observe that the hysteresis behaviour remains clear for flow surface elevation and mean force against force power (Figure S6a-b and Figure S6d-e), while the rising and falling limbs of volumetric solid concentration collapse on a unique curve (Figure S6c and Figure S6f). These observations confirm that the small clockwise hysteresis showed in Figure 3b and Figure 3f is not significant.

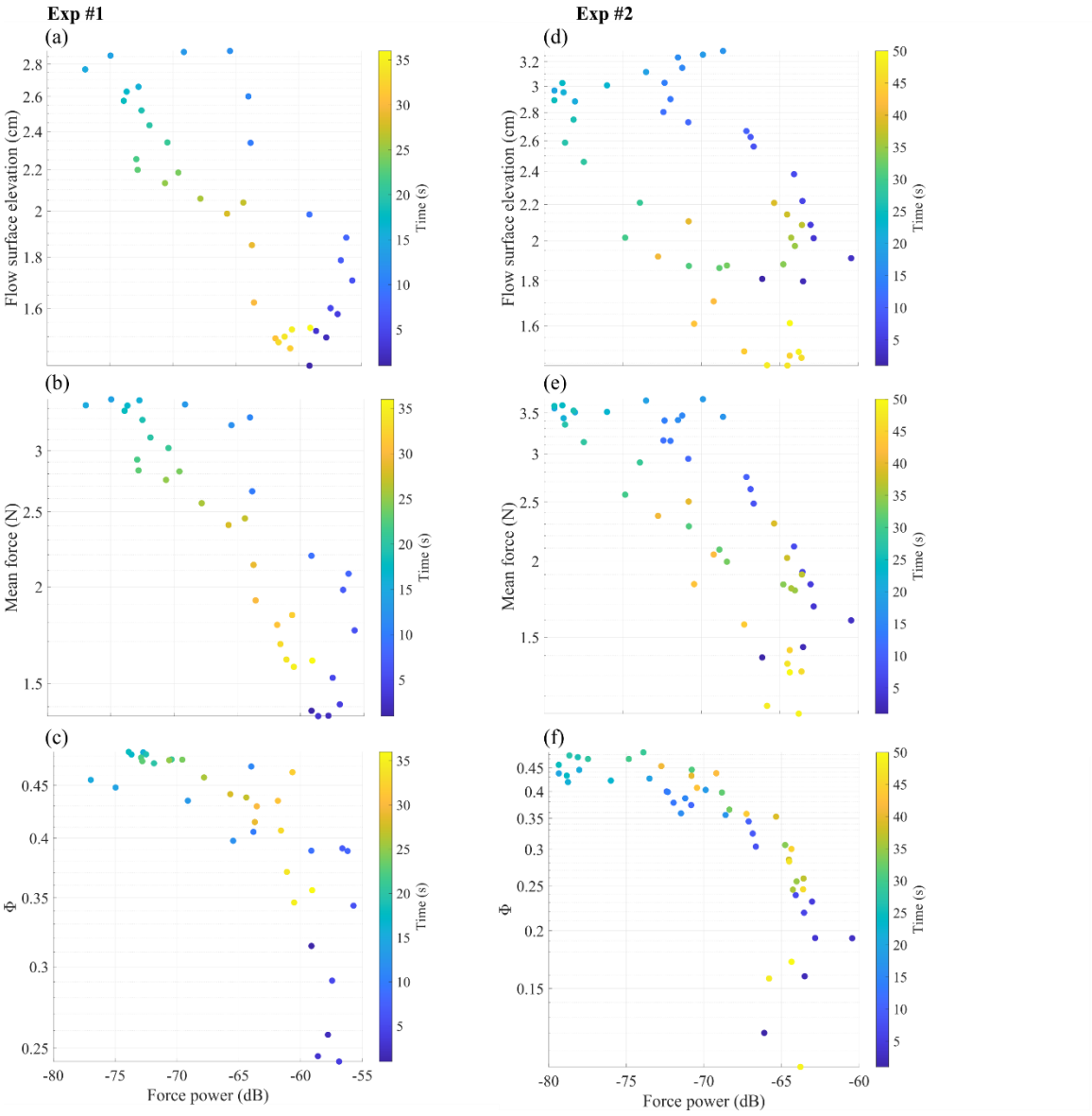

Figure S6. All the panels of Figure S6 refer to the time intervals between the vertical dashed red lines in Figure 2f and 2j. The log-log scatterplots of Figure S6a-b-c and Figure S6d-e-f have force power on the x axis and flow properties on the y axis, where dots' color changes with time. All the measurements are smoothed on a time window of 2 sec.

Movie S1. Movie S1 is from the webcam installed above the force plate. It refers to Exp #2.

Movie S2. Movie S2 is from the camera installed close to the upstream piezoelectric sensor. It refers to Exp #2.